Supplementary Material for

Microcage flame retardants with complete recyclability and durability via reversible interfacial locking engineering

Furong Zeng, Lei He, Jianwen Ma, Danxuan Fang, Zhiwei Zeng, Tongyu Bai, Rong Ding, Bowen Liu, Haibo Zhao*, Yuzhong Wang*

School of Chemical Engineering, The Collaborative Innovation Center for Eco-Friendly and Fire-Safety Polymeric Materials (MoE), National Engineering Laboratory of Eco-Friendly Polymeric Materials (Sichuan), State Key Laboratory of Polymer Materials Engineering, Sichuan University

No. 24, South Section 1, Yihuan Road, Chengdu, Sichuan 610064 (China)

*Correspondence to: haibor7@163.com, polymers@vip.126.com.

This PDF file includes:

1. Experimental section
2. Figure S1-S40
3. Table S1-S10
4. References 1-18

1. Experimental section

1.1 Materials

Diphenylphosphinic acid (PA), potassium propionate (PK), diglycidyl ether (DGEBA), and 4,4'-diaminodiphenylmethane (DDM) were obtained from Aladdin Biochemical Technology Co., Ltd. (Shanghai, China). Copper chloride dihydrate ($CuCl_2 \cdot 2H_2O$, CC), sodium hydroxide (NaOH), concentrated hydrochloric acid (HCl, 36-38%), urea, sodium chloride (NaCl), N,N-dimethylformamide (DMF), sodium dodecyl sulfate (SDS), absolute ethanol (EtOH), dichloromethane (DCM), and ethylene glycol were obtained from Kelong Chemical Reagent Corp. (Chengdu, China). Polyether polyols (GEP-560s) were obtained from Gaoqiao Petrochemical Company (Shanghai, China). The corresponding average molecular weight and average functionality are 3000 and 3.0, respectively, and the -OH content is 56 mg of KOH/g. Toluene diisocyanate (TDI 80/20, technically pure grade) was obtained from Chengdu Gaoduan Polymer Technology Co., Ltd. (Chengdu, China). The catalysts (stannous octoate, T9; 33% triethylenediamine solution, A33) and surfactant (SZ 580) were kindly supplied by Chengdu Ruijie Co., Ltd. (Chengdu, China). Deionized water was used as the chemical blowing agent. All the reagents were used without further purification. Commercial polycarbonate (PC) was obtained from Daphoon.

1.2 Characterizations

Spectroscopic and morphological characterization: Fourier transform infrared (FT-IR) spectroscopy was performed with a Nicolet 6700 instrument. The ultraviolet and visible (UV–vis) spectra were measured between 200 and 800 nm using a Cary 50 spectrophotometer (Agilent) and a UV-3600i Plus (Shimadzu). X-ray photoelectron spectroscopy (XPS) was performed on a K-Alpha spectrometer (Thermo Fisher Scientific) equipped with Al Kα excitation radiation. The data were processed using CasaXPS software, and the energy was calibrated to the C 1s peak at 284.8 eV. X-ray powder diffraction (XRD) was performed on a Bruker-D2 PHASER Powder X-ray Diffractometer equipped with Cu radiation (l ¼ 1.542 E), and the scanning speed over

2θ ranging from 5° to 60° was 6° min^{-1}. Elemental analysis (EA) was carried out on a Flash EA 1112 analyzer for carbon, hydrogen, and oxygen. Inductively coupled plasma optical emission spectroscopy (ICP–OES) was performed on a 5100 SVDV (Agilent) for phosphorous. Scanning electron microscopy (SEM) images, elemental mappings, and energy dispersive spectroscopy were obtained on a Phenom ProX scanning electron microscope (Phenom World). Nuclear magnetic resonance (NMR) spectra were obtained on a Bruker AVIII400 HD spectrometer (DMSO-d$_6$). The number-averaged molecular weight (M_n), weight-averaged molecular weight (M_w), and molecular weight distribution (M_n/M_w, Đ) were determined by an HLC-8320 GPC apparatus (Dongcao) equipped with a refractive index detector. All the calibrations were performed by using polystyrene as the standard. Tetrahydrofuran was used as the eluent at a flow rate of 0.6 mL min^{-1} at 40 °C.

Mechanical performance: The compression and resilience properties of PUF were characterized by a universal testing machine (Instron 5400) equipped with 500 N load cells at 50% compression deformation and a strain rate of 20 mm min^{-1}. The mechanical resilience was evaluated according to ISO 1856-2000 with a sample size of 50 mm × 50 mm × 25 mm. The samples were maintained at 70 °C for 22 h with 50% compression deformation. The density was calculated by the volume and weight of the flame-retardant materials according to ISO 845:2006.

Characterization of thermostability and durable flame retardancy: Thermogravimetric analysis (TGA) was performed using a NETZSCH TG 209 F1 instrument at a heating rate of 10 °C min^{-1} from 40 °C to 700 °C under N$_2$ (50 mL min^{-1}). TG-MS was performed on a STA449F5-QMS403 (NETZSCH) at a linear heating rate of 10 °C min^{-1} from 40 °C to 700 °C under nitrogen flow (50 mL min^{-1}). TG-IR spectra were analyzed by a PerkinElmer STA6000-Frontier at a heating rate of 20 °C min^{-1} from 40 °C to 700 °C in a N$_2$ atmosphere. According to GB/T 2406.2-2009, the limiting oxygen index (LOI) of samples with a size of 10 mm × 10 mm × 150 mm were measured by an HC-2C oxygen index meter (Jiangning). Vertical burning tests (VBT) of samples suspended vertically in the cabinet were performed based on the California

Technical Bulletin (Cal TB 117). The durable flame retardancy of PUF was demonstrated by accelerated aging tests conducted by hydrothermal aging (105 °C for 3 h with 100% humidity) based on GB/T 9640-2008. Correspondingly, LOI and VBT experiments were performed on the original EP&PC and flame-retardant samples aged for 12 h in water at 60 °C. In addition, according to ISO 5660-1, the combustion performance of the samples was assessed on a cone calorimeter device (Fire Testing Technology), and specimens with a size of 100 mm × 100 mm × 25 mm were exposed to a heat flux of 25 kW/m^2.

Simulations: The interactions of two PA molecules with different mediators (H_2O and EtOH) were evaluated via density functional theory (DFT), in which all the structures were optimized via Gaussian 09 E.01[1] with fine integration grids at the Lee-Yang-Parr gradient-corrected correlation functional (B3LYP) hybrid functional [2] and the 6-31+G (d,p) basis set. Grimme's D3BJ dispersion correction was combined with the B3LYP functional. Harmonic frequencies were applied at the same level to verify that the structure after optimization corresponded to the minima on the potential energy surface. The binding energy (BE) of the two monomers was calculated as follows:

$$E_{dimer} = E_{total} \text{-} E_{monomer1} \text{-} E_{monomer2}$$

where E_{dimer}, $E_{monomer1}$, and $E_{monomer2}$ are the total energy of the two PA monomers, the single point energy of monomer 1, and the single point energy of monomer 2, respectively. The more negative the magnitude of the interaction energy is, the more favorable the interaction is. Water and ethanol implicit solvents were considered in all calculations via a solvation model based on solute electron density (SMD). The molecular electrostatic potential and coordination structure were optimized via Gaussian 09 E.01. The B3LYP method with the 6-31G (d, p) basis was used for C, H, O, and P; atoms; and the lanl2dz basis was used for Cu atoms. The use of an ethanol implicit solvent was considered in all calculations via a solvation model based on SMD.
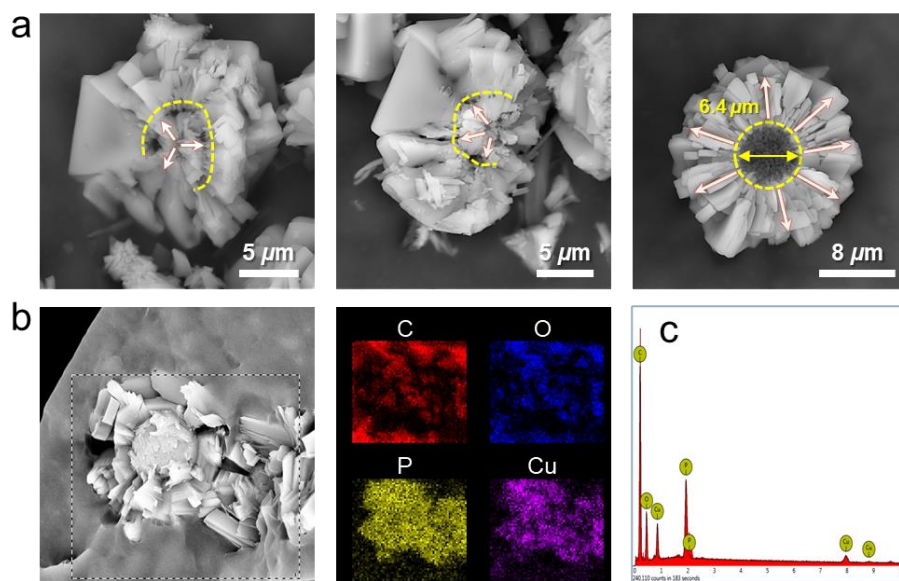
2. Figure S1-S39

Figure S1. Morphology analysis for the hierarchal structures in PM. (a) Localized SEM images, (b) corresponding elemental mappings, and (c) energy dispersive spectroscopy for the cross section of PM.
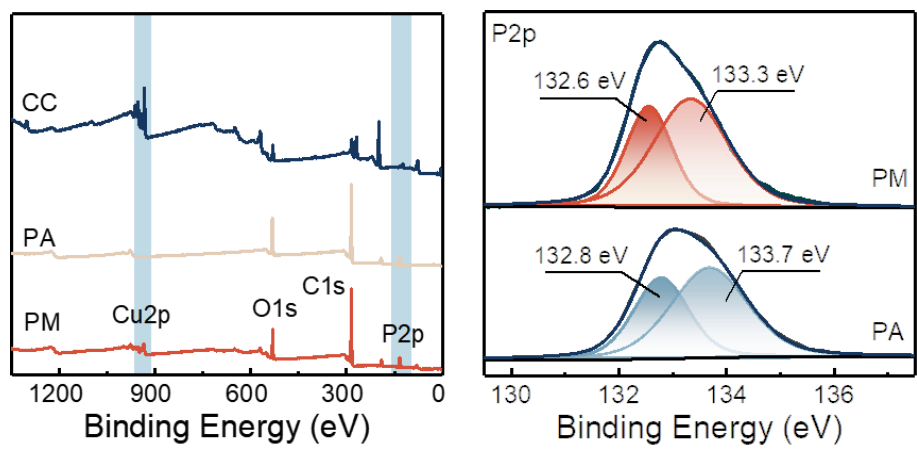
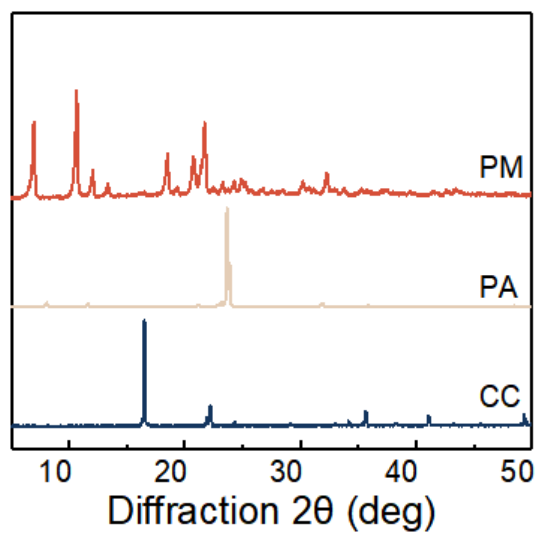**Figure S2.** XPS spectrum and high-resolution P 2p spectrum of PM.
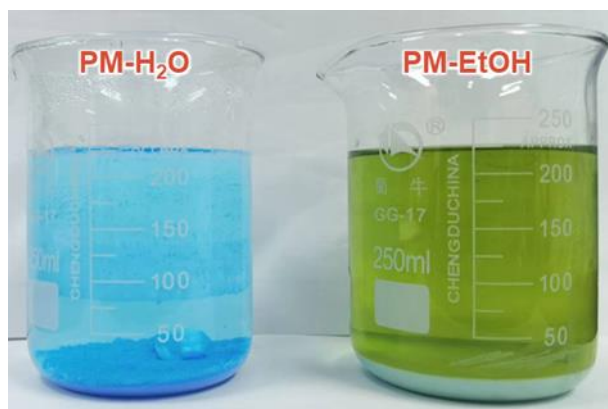
Figure S3. XRD patterns of PM, PA, and CC.

Figure S4. Photographs of the precipitates for PM-H$_2$O (H$_2$O as the sole solvent) and PM-EtOH (EtOH as the sole solvent) after being incubated for 1 h. Notably, upon the addition of the Cu^{2+} solution, PM-EtOH was generated more rapidly than PM-H$_2$O.
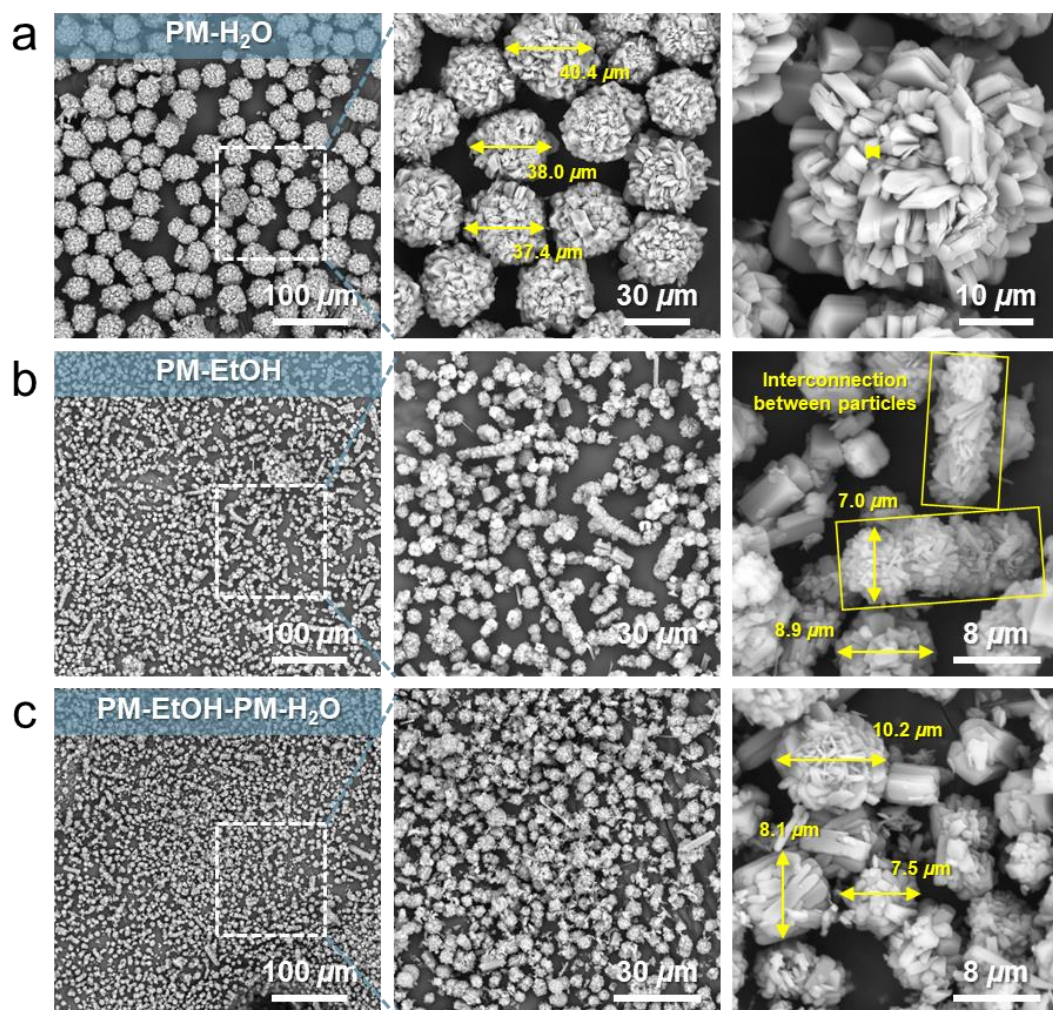
Figure S5. SEM images of (a) PM-H_2O, (b) PM-EtOH, and (c) PM-EtOH-H_2O (obtained by washing PM-EtOH with H_2O to remove the byproduct NaCl).
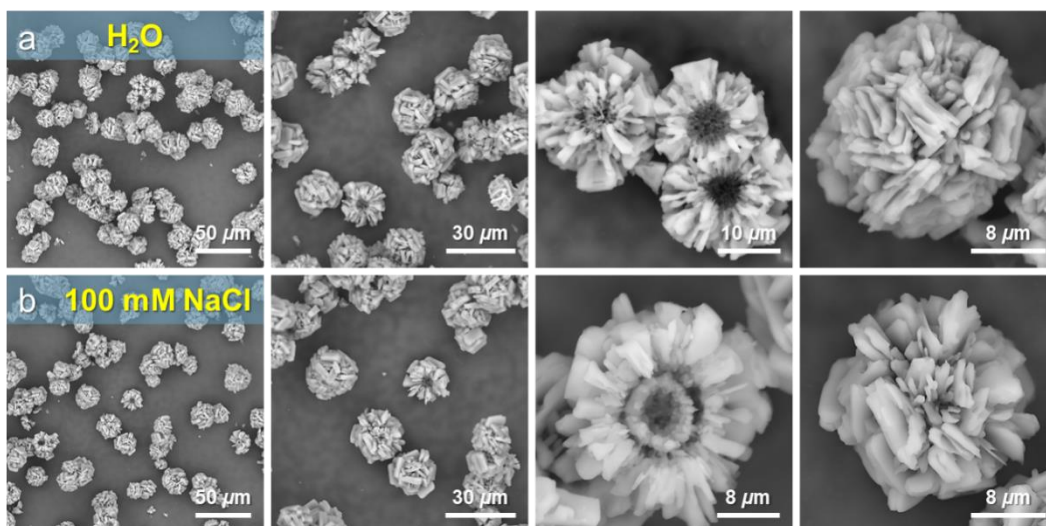
Figure S6. Representative SEM images of PM after incubation in (a) H_2O and (b) 100 mM NaCl aqueous solution for 30 min.
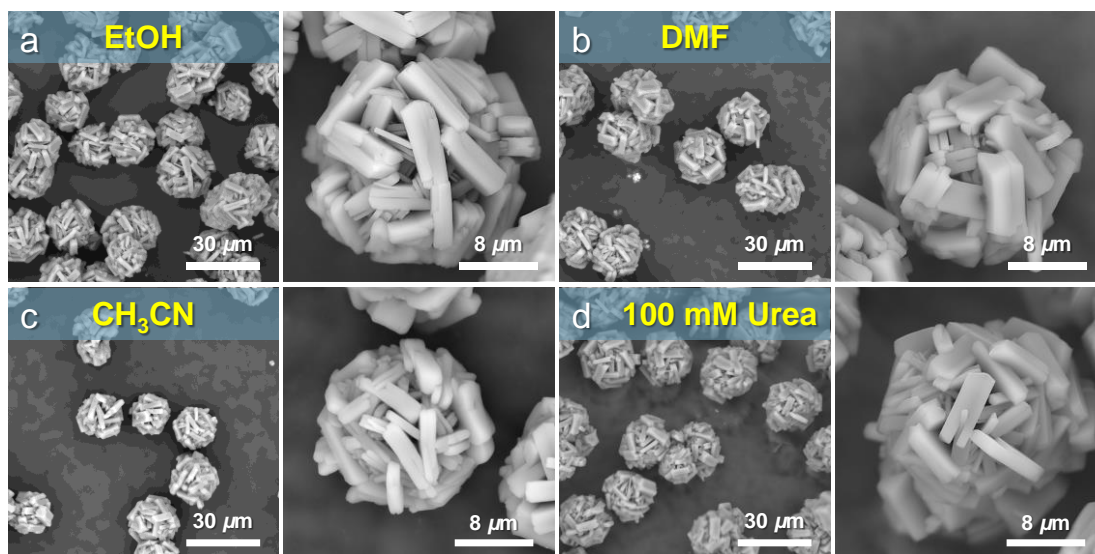
Figure S7. Representative SEM images of PM after incubation in (a) EtOH, (b) DMF, (c) CH_3CN, and (d) 100 mM urea aqueous solution for 30 min.
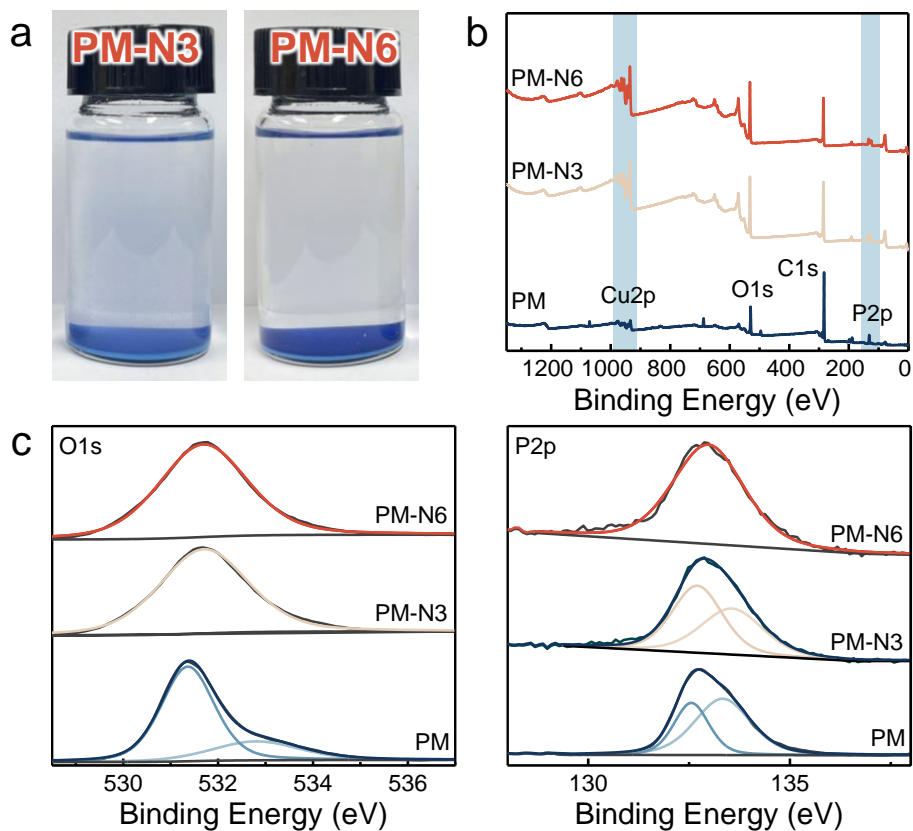
Figure S8. (a) Photographs of PM dispersions after incubating in 50 mM NaOH ethanol solution for 30 min and 60 min, respectively. (b) XPS spectra and (b) high-resolution P 2p & O 1s spectra of PM, PM-N3, and PM-N6, respectively.
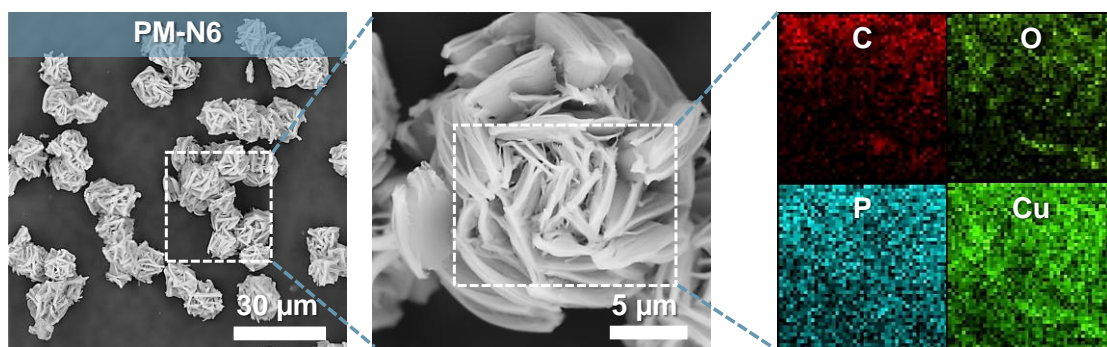
Figure S9. SEM images and the corresponding elemental mappings of PM-N6.
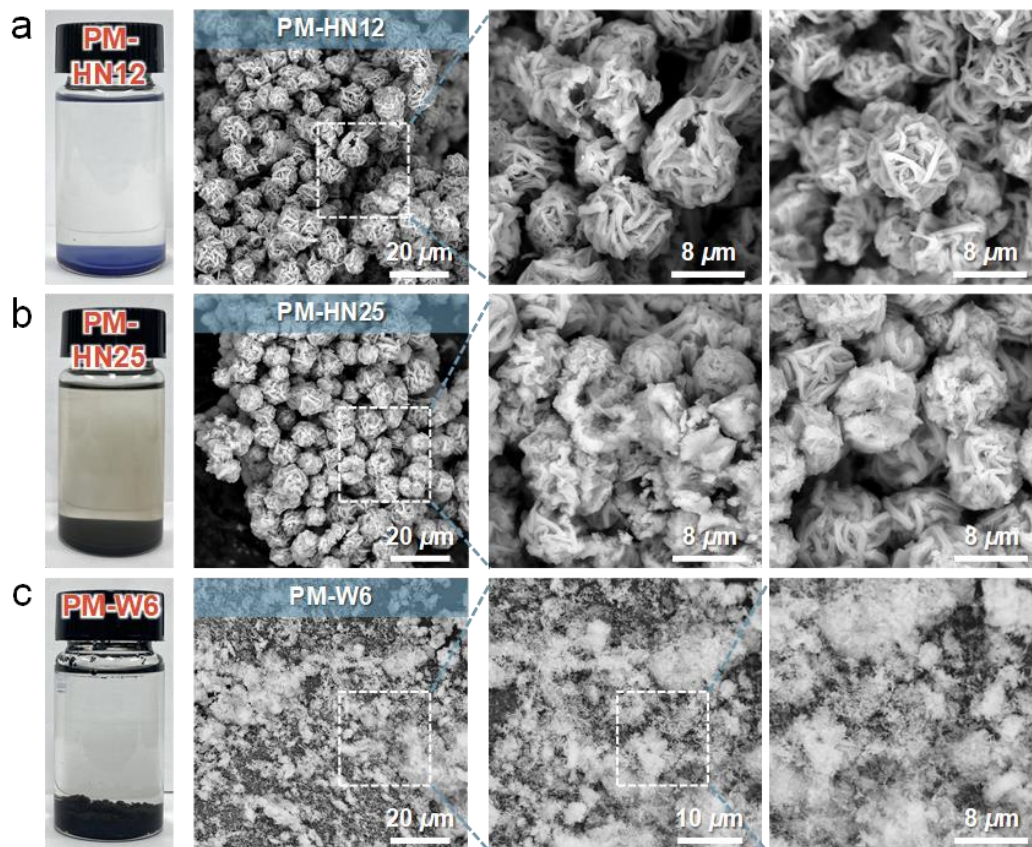
Figure S10. Photographs and SEM images of PM after incubation in (a) 120 mM NaOH ethanol solution for 22 h, (b) 250 mM NaOH ethanol solution for 60 min, and (c) 50 mM NaOH aqueous solution for 60 min.
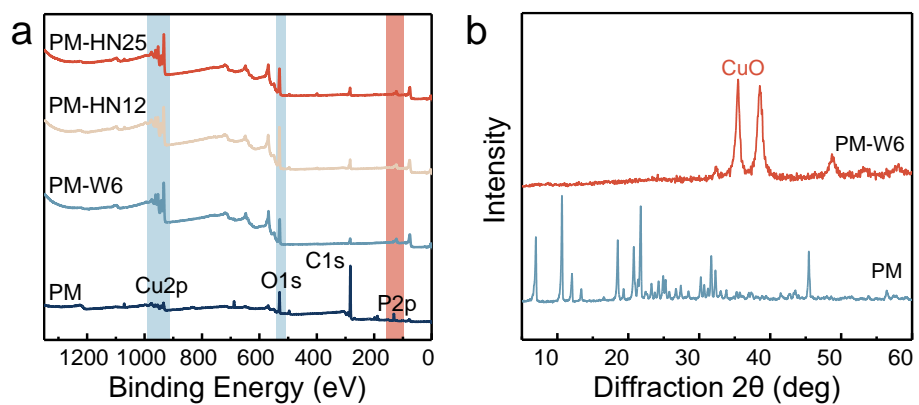
Figure S11. (a) XPS spectra of PM, PM-W6, PM-HN12, and PM-HN25. (b) XRD patterns of PM and PM-W6.
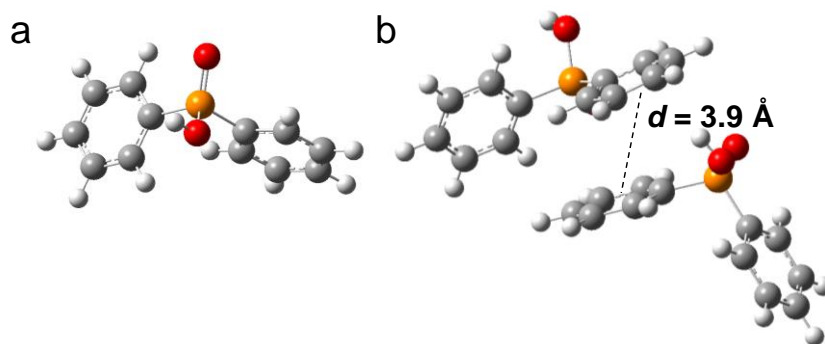
Figure S12. (a) Initial structure of PA. (b) Optimized structure showing the molecular details of aromatic stacking in H_2O. Carbon, oxygen, hydrogen, and phosphorus are colored gray, red, white, and purple, respectively.
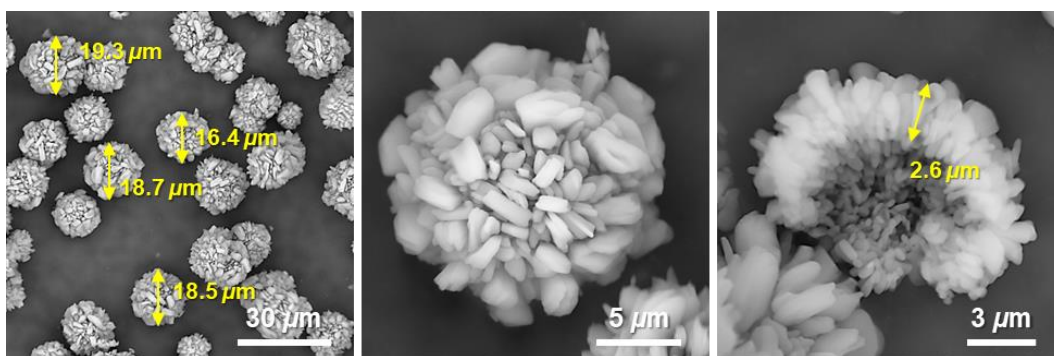
Figure S13. Morphological transition of PM incubated with a small volume of HCl ethanol solution (0.1 M).
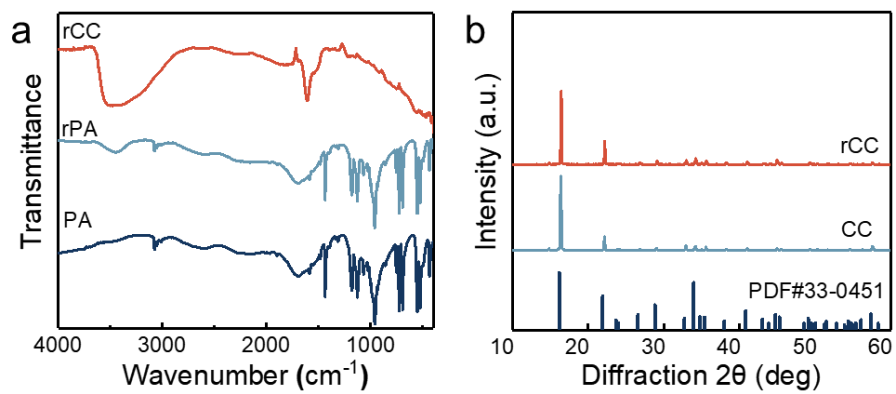
Figure S14. Structural characterization of the starting monomers and recovered assembly precursors. (a) FT-IR spectra and (b) XRD patterns of rPA and rCC.

Figure S15. SEM images of the brittle fracture of neat foam (N-F) and flame-retardant foams (PM-F) with PM.

Figure S16. ^{13}C NMR and ^{31}P NMR spectra of the recovered raw materials rPA-F and rCC-F obtained from PM-F.

Figure S17. FT-IR spectra of the recovered raw materials rPA-F and rCC-F obtained from PM-F.

The direct degradation and reuse of foam waste embedded with flame retardants will cause impurities in the recovered polyols and worsen the perfor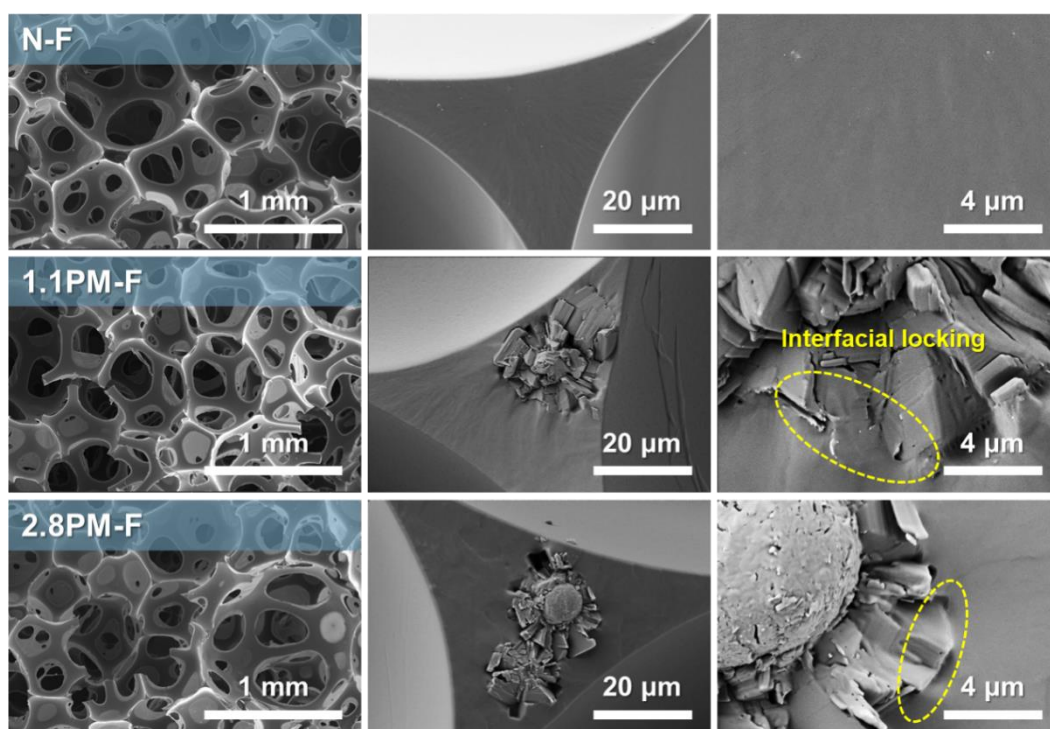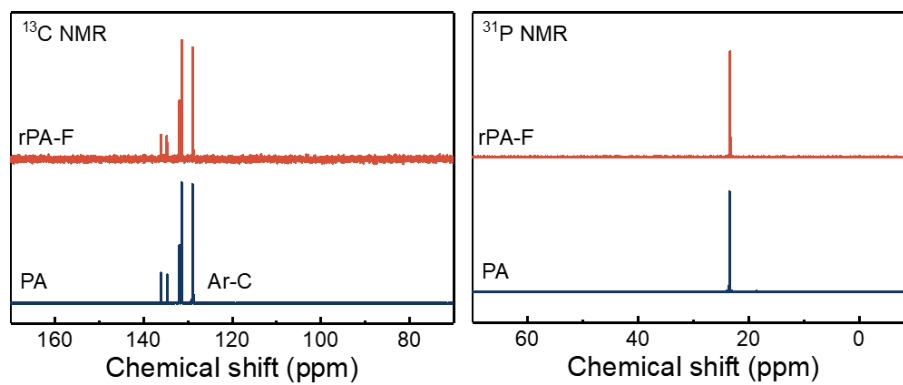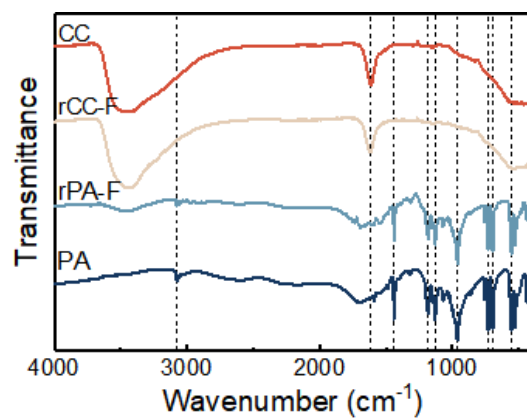mance of the regenerated materials. In particular, the impacts of metal-containing compounds, which are widely used as catalysts in a considerable portion of organic matter and for polymer polymerization, on the degradation process of polymers have not been fully elucidated. Fortunately, the chemical degradation of foam can proceed as a neat PUF after removing PM. To demonstrate feasibility, glycolysis was used to gain insight into the impacts of PM on the chemical recycling process of foams. Derived from the aromatic segments of the isocyanate used in polyurethane, undesirable amine-functionalized products inevitably formed during glycolysis. As shown in **Figure S19a-b**, the hydrolysis of urethane bonds occurs in parallel with the glycolysis reaction in the presence of water derived from glycolizing agent or polyurethane, resulting in amine-functionalized polyols and thus leading to a greater hydroxyl number than that of the starting polyol.[3-5] In addition, as shown in **Figure 3k** and **Figure S20**, strong peaks assigned to C-H and C-O-C in the FT-IR spectra and proton signals attributed to $-CH_3$ (0.9-1.1 ppm) and $O-CH-CH_2-$ (3.3-3.6 ppm) in the NMR spectra demonstrated that the main ingredients of the recycled polyols were the raw polyols.

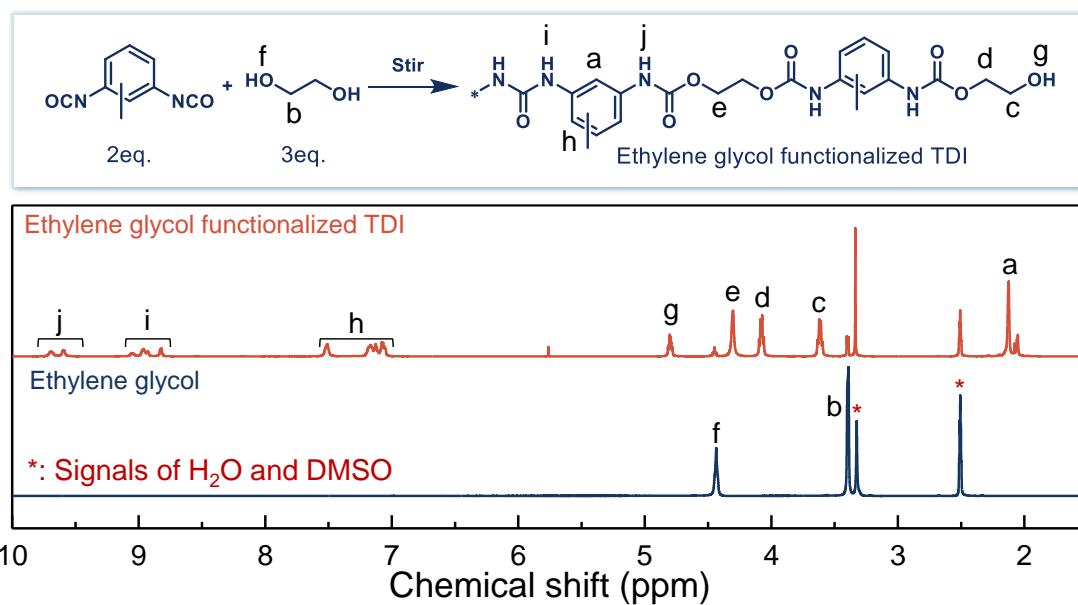**Figure S18.** Model reaction of ethylene glycol with toluene diisocyanate (TDI 80/20) at room temperature for 3 h at a molar ratio of 3/2 and the corresponding assignment of characteristic signals of ethylene glycol and the crude reaction mixture, i.e., ethylene glycol-functionalized TDI. Model reactions of small molecules were carried out to assess the molecular information of the recycled polyols.

a

Ethylene glycol functionalized polyols   Amine functionalized polyols

↑ R: Main chain of GEP-based polyols   ↓ *: Signals of ethylene glycol, H_2O, and DMSO

Recycled polyols	Catalysts	CH_3*-C(O)- [b]	-O-CH_2*-CH_2-OH (×100)	-(CO)-NH*-Ph- (×10)	CH*(Ph) (×10)
PN-FK	1 wt%	1	0.06	0.01	0.07
PPM-FK	Potassium	1	0.96	0.11	0.31
PvPM-FK	propionate [a]	1	0.01	0.00	0.02

a) Related to the foam mass by weight, b) the integral area of C-H (signal a) in polyols is used as reference.
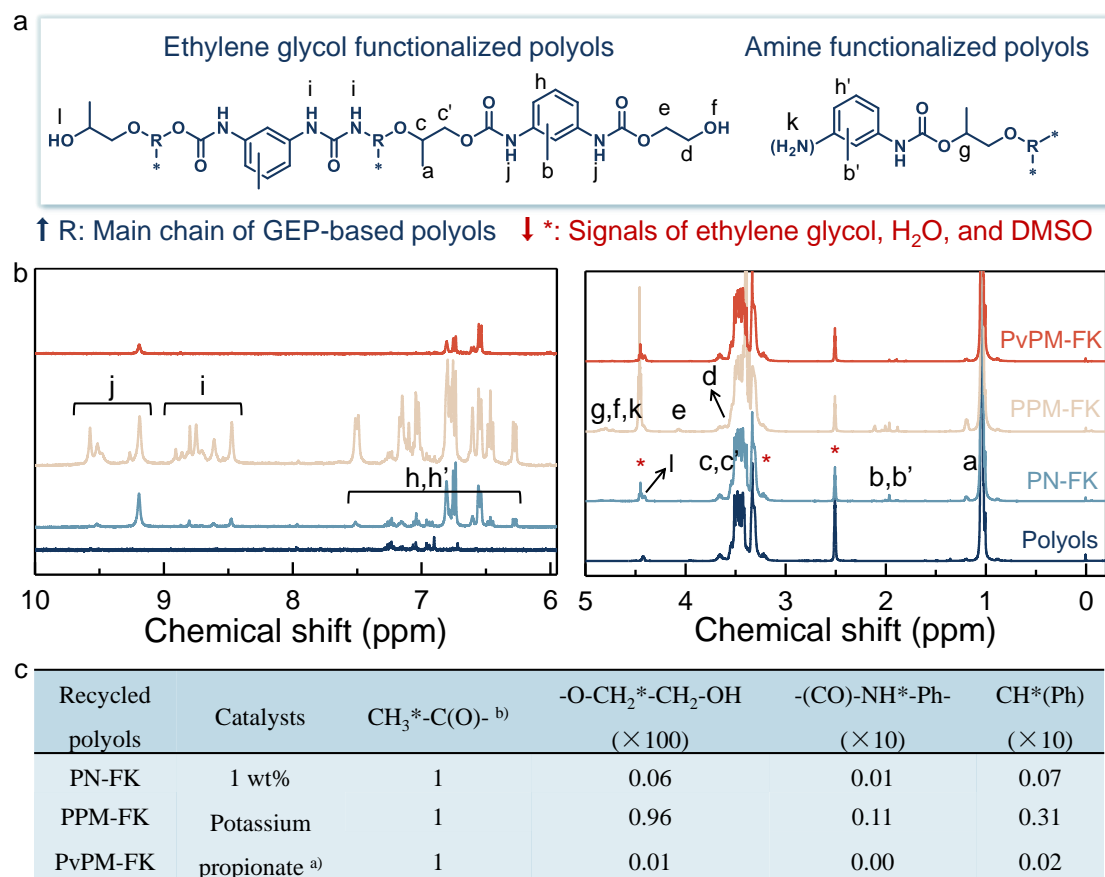
Figure S19. Assignment of characteristic signals of recycled polyols obtained by glycolysis from foams with 1 wt% potassium propionate. (a) Chemical structures and (b) magnified ^{1}H NMR spectra of recycled polyols. (c) Integral area of selected H protons in recycled polyols.
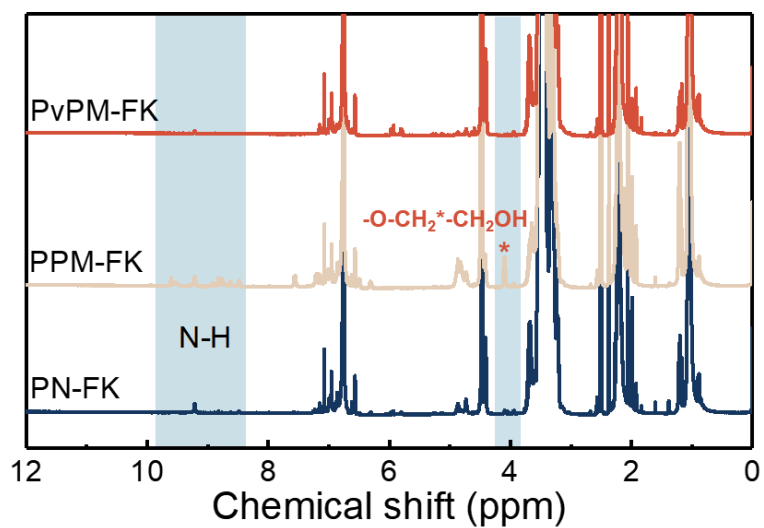
Figure 20. Content of amine (-NH) groups was determined by ^{1}H NMR spectroscopy of recycled polyols obtained by glycolysis of PUF with 1 wt% potassium propionate. (Mesitylene was used as an internal standard.)

The remaining contents of P and Cu in recycled polyols PPM-F reached 22.7% and 6.6%, respectively, without potassium propionate as a catalyst, while PvPM-F and PN-F had barely detectable P or Cu-containing impurities, as shown in **Table S5** and **Figure S21**. Correspondingly, PN-F, PPM-F, and PvPM-F exhibited identical molecular weights/distributions and strong C=O and N-H peaks (**Figure S22-24**). The foam matrix degraded more thoroughly as the catalyst dosage increased from 0 to 1 wt%, leading to gradual weakening of the proton signals for NH, O-CH$_2$*-CH$_2$OH, and Ph-H, as shown in **Figure S25**. However, PPM-F1K exhibited a remarkably greater content of O-CH$_2$*-CH$_2$OH (0.98) than did PN-FK (0.06), even with a 1 wt% base catalyst, similar to that of PN-F without a catalyst (0.92) (**Figure S19c** and **Figure S25**).
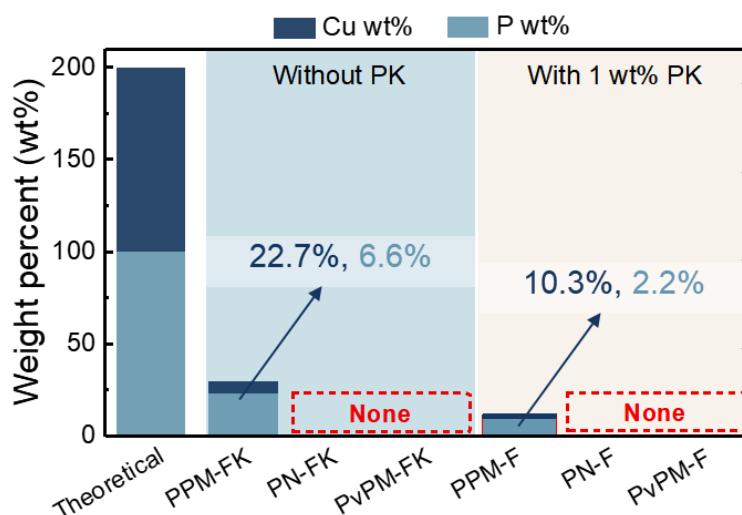
Figure S21. Contents of phosphorus and copper in recycled polyols obtained by glycolysis of PUF with or without potassium propionate.

Figure S22. Photographs of the chemical recycled polyols (upper phase) from (a) N-F, (b) PM-F, and (c) vPM-F without potassium propionate.

Figure S23. (a) GPC traces and (b) FT-IR spectra of polyol GEP 560 s and recycled polyols (PN-F, PPM-F, and PvPM-F) obtained by glycolysis of PUF without potassium propionate.

a

	N-H		C-H(Ar)			-CH₂-			

PPM-F1PK

PPM-F0.1PK

PPM-F0PK

Chemical shift (ppm)

b

Recycled polyols	Potassium propionate [a]	CH₃*-C(O)-[b]	-O-CH₂*-CH₂-OH (×100)	-(CO)-NH*-Ph- (×10)	CH*(Ph) (×10)
PPM-F0K	/	1	1.33	0.17	0.41
PPM-F0.1K	0.1 wt%	1	1.24	0.16	0.40
PPM-F1K	1.0 wt%	1	0.98	0.11	0.31

a) The weight percent of catalyst potassium propionate is related to the foam mass, and b) the integral area of C-H in polyols is used as reference
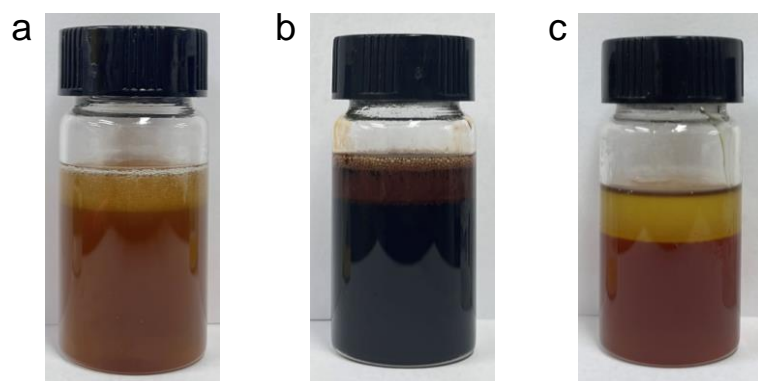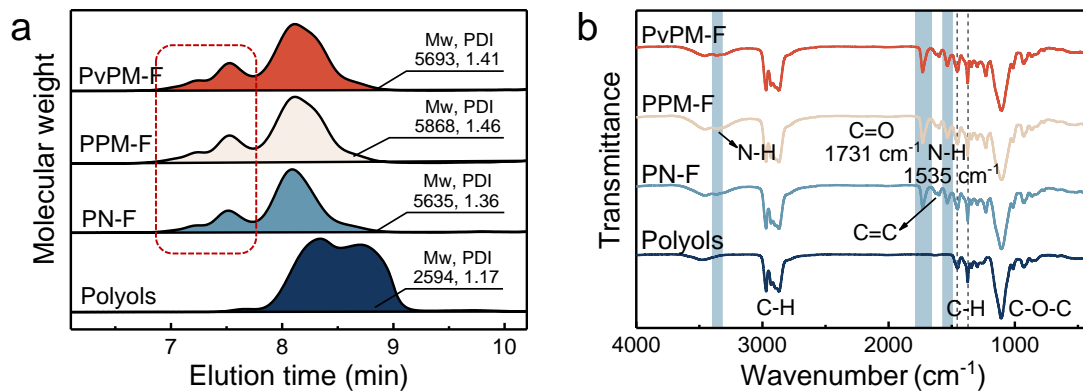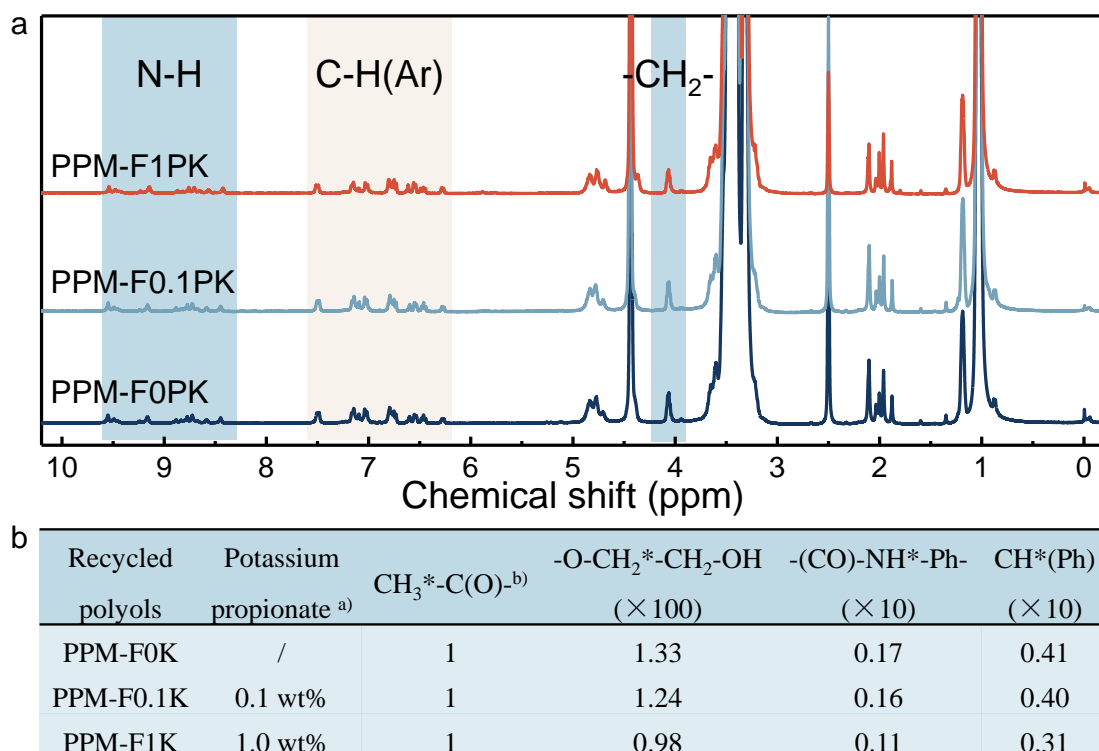
Figure S24. Assignment of characteristic signals of recycled polyols obtained by glycolysis of PUF with different potassium propionate loadings. (a) Magnified ¹H NMR spectra of the recycled polyols. (b) Integral area of selected H protons in recycled polyols.
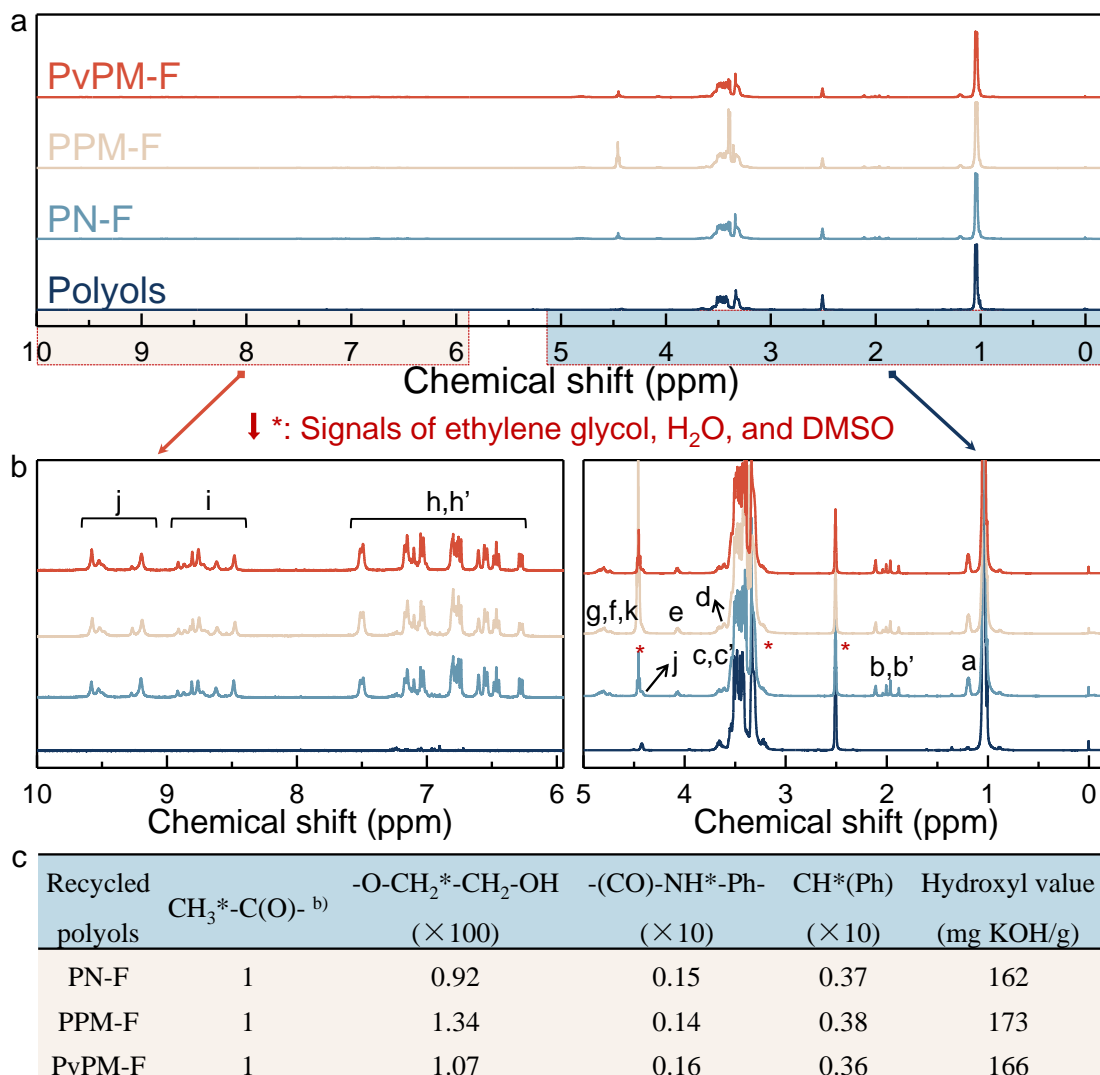
Figure S25. Assignation of characteristic signals of recycled polyols obtained by glycolysis of PUF without potassium propionate. (a-b) Magnified ^{1}H NMR spectra of recycled polyols. The characteristic signals are assigned to the corresponding protons, and the chemical structures are shown in **Figure S20a**. (c) Integral area of selected H protons and the hydroxyl value of recycled polyols.

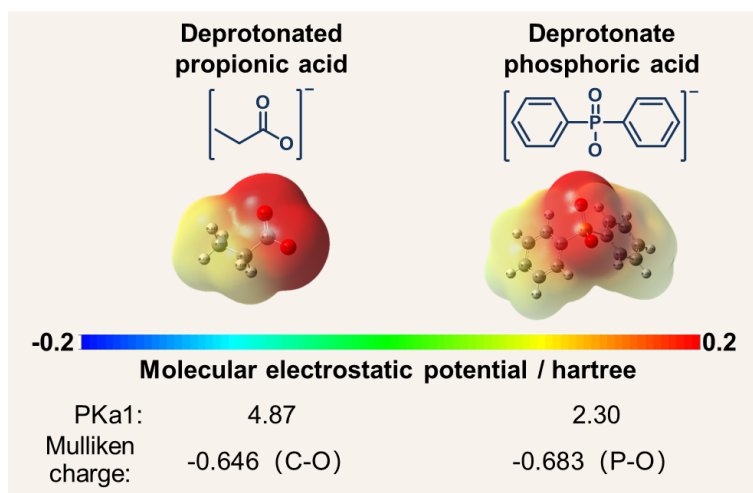| Recycled polyols	CH_3*-C(O)- [b)	-O-CH_2*-CH_2-OH ($\times$100)	-(CO)-NH*-Ph- ($\times$10)	CH*(Ph) ($\times$10)	Hydroxyl value (mg KOH/g)
PN-F	1	0.92	0.15	0.37	162
PPM-F	1	1.34	0.14	0.38	173
PvPM-F	1	1.07	0.16	0.36	166

Figure S26. Comparison of the molecular electrostatic potentials of deprotonated propionic acid and phosphoric acid and the Mulliken charges of C-O in propionic acid and P-O in phosphoric acid.
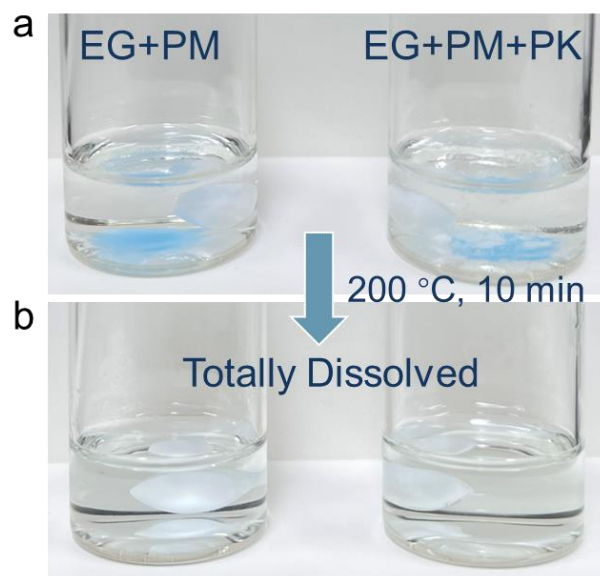
Figure S27. Digital images of EG dispersions of 10 g EG+10 mg PM and 10 g EG+10 mg PM+100 mg PK showing dissolution states (a) before and (b) after stirring at 200 °C for 10 min.
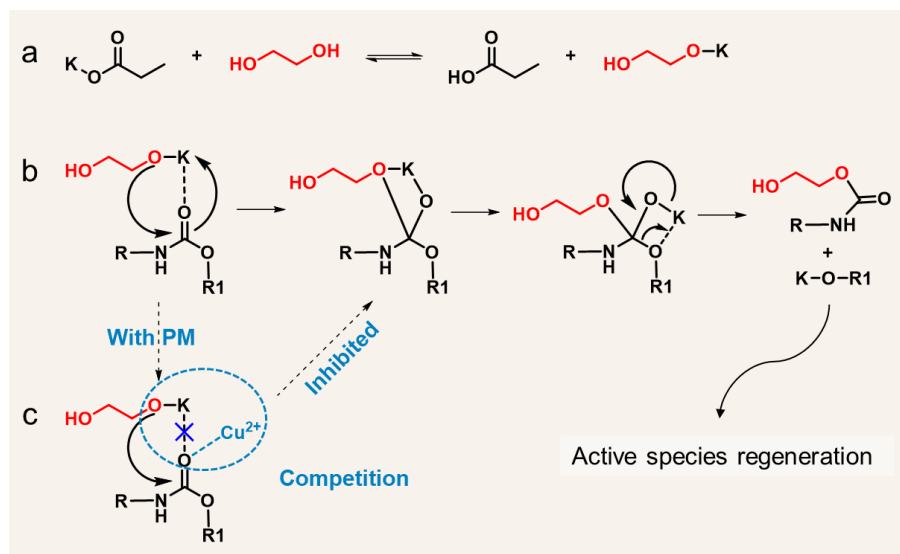
Figure S28. Proposed mechanism of recycling process of glycolysis. (a) Initiator alkoxide formation. (b) Coordination/insertion and exchange. (c) Chemical recycling of foams in the presence of PM.
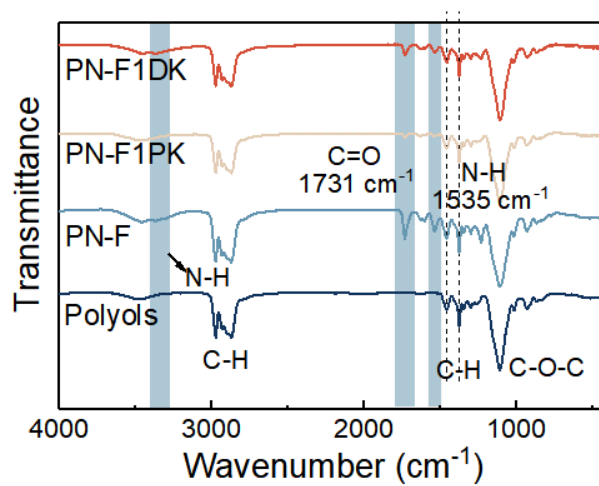
Figure S29. FT-IR spectra of polyols and recycled polyols (PN-F, PN-F1PK, and PN-F1DK) obtained by glycolysis of N-F without or with different catalyst (e.g., PK and DK).
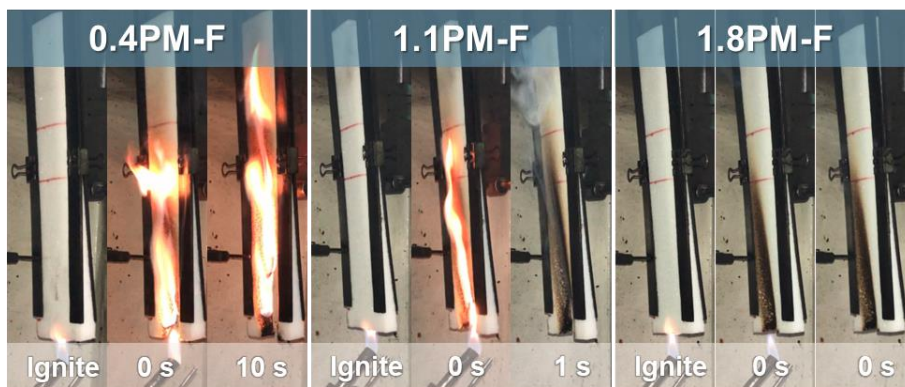
Figure S30. Digital photographs at different burning times of PM-F with 0.4 wt%, 1.1 wt%, and 1.8 wt% PM, respectively.
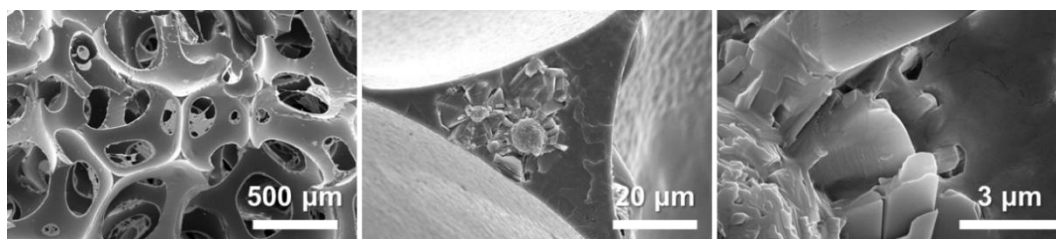
Figure S31. SEM images for the brittle fracture of aged 2.8PM-F.
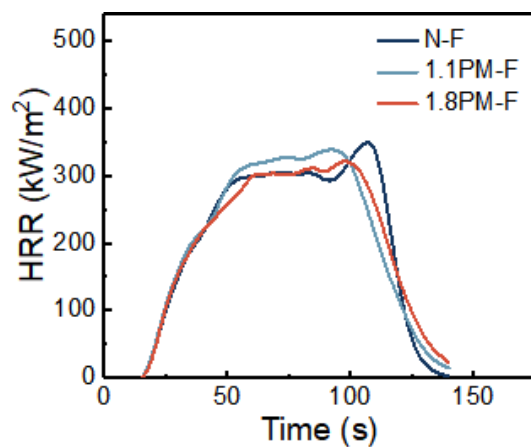
Figure S32. Heat release rate (HRR) curves of neat F and PM-F at a heat radiation of 25 kW/m^2.
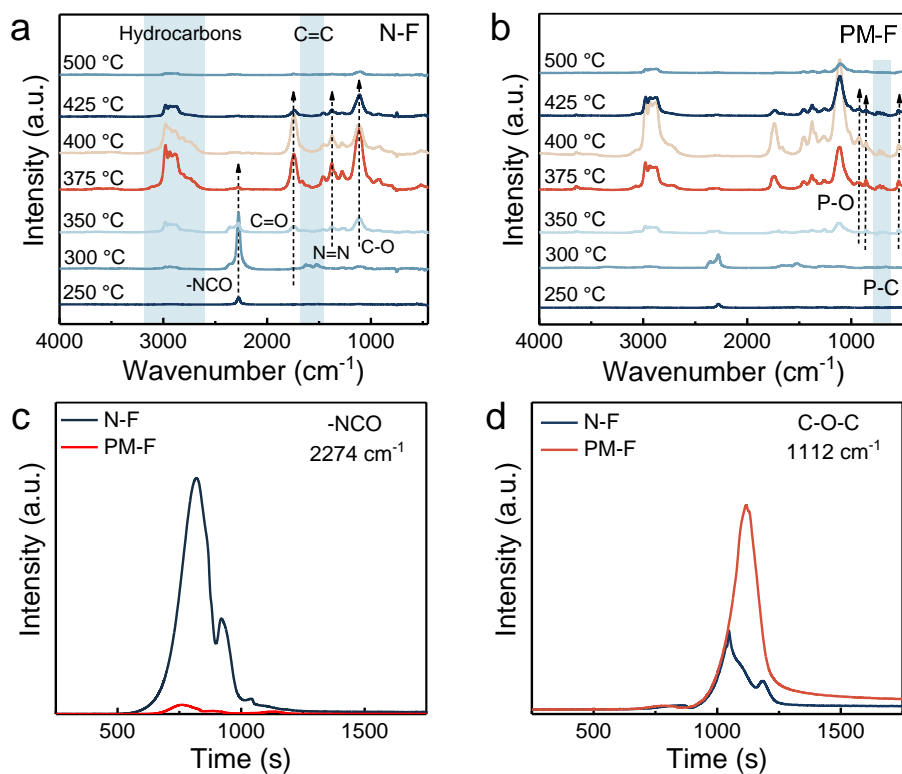
Figure S33. FT-IR of the gaseous decomposition products of (a) N-F and (b) PM-F tracked by TG-IR. (c-d) Selected gaseous decomposition products as a function of time derived from the pyrolysis process.
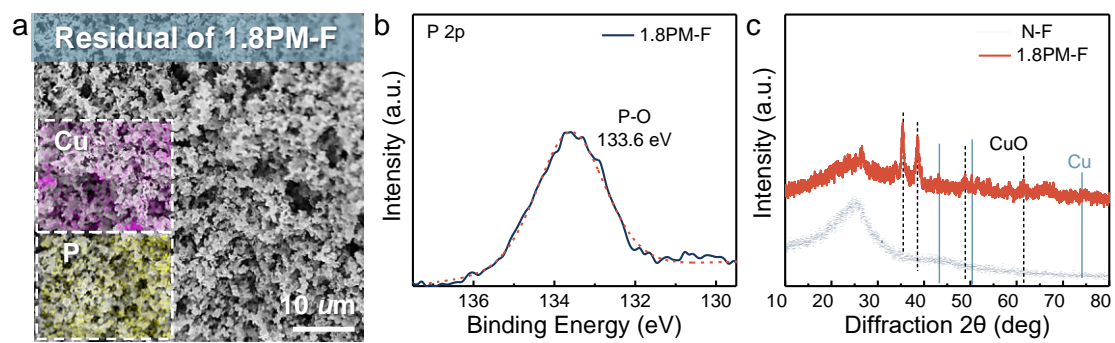
Figure S34. (a) SEM image and elemental mappings, (b) high-resolution P 2p spectra, and (c) XRD patterns of the residues of N-F and PM-F after cone calorimetry.
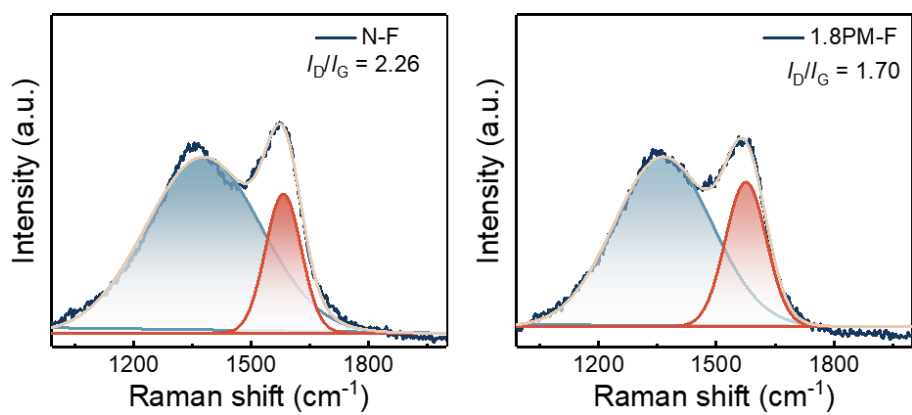
Figure S35. Raman spectra of the N-F and PM-F residues after cone calorimetry.
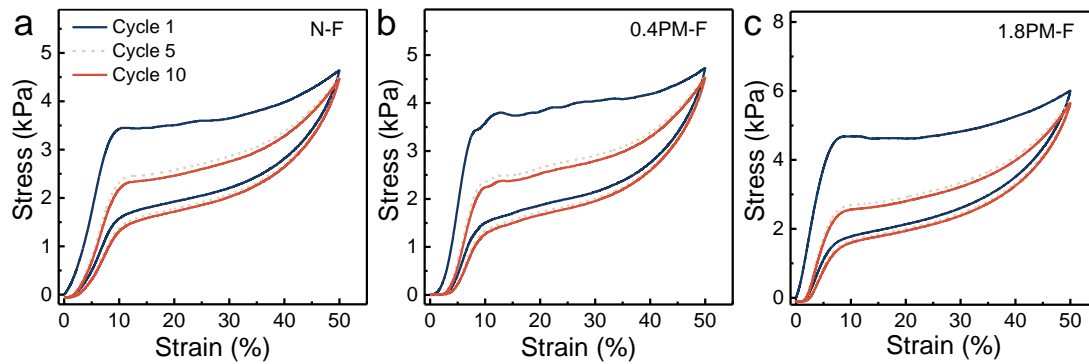
Figure S36. Compressive cyclic stress–strain curves of N-F and PM-F.
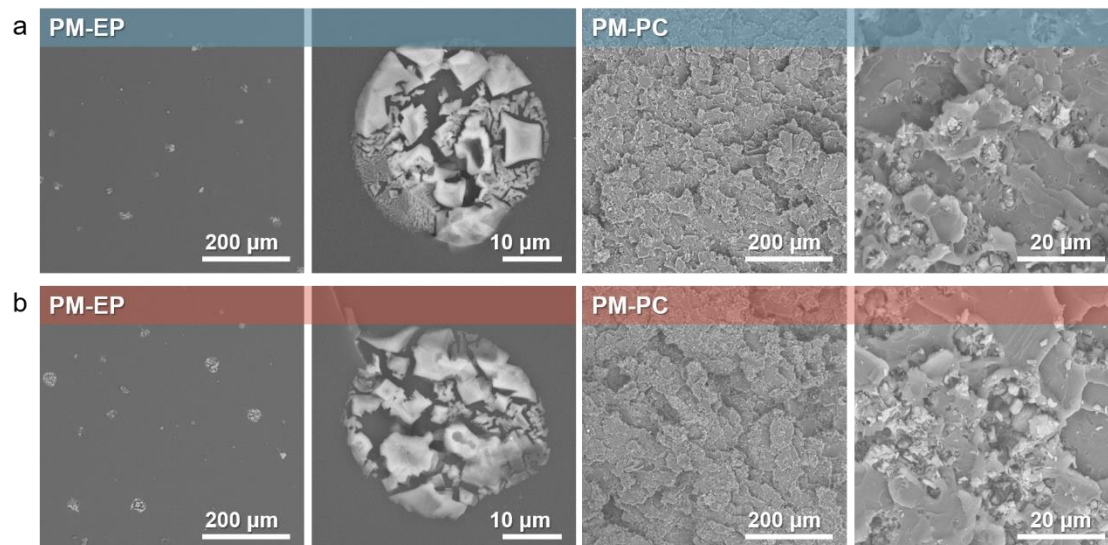
Figure S37. SEM images of flame-retardant EP and PC (a) before and (b) after incubation in hot water.

PMs were intimately embedded in the matrix of EP via robust interfacial locking without visible phase interfaces, showing high compatibility. Due to the high pressure during the preparation process, the microcage-like structures of PM were crushed but still uniformly distributed in PC. After exposure to hot water, the corresponding morphology remained intact and consistent with that before exposure, indicating excellent resistance to hot water.
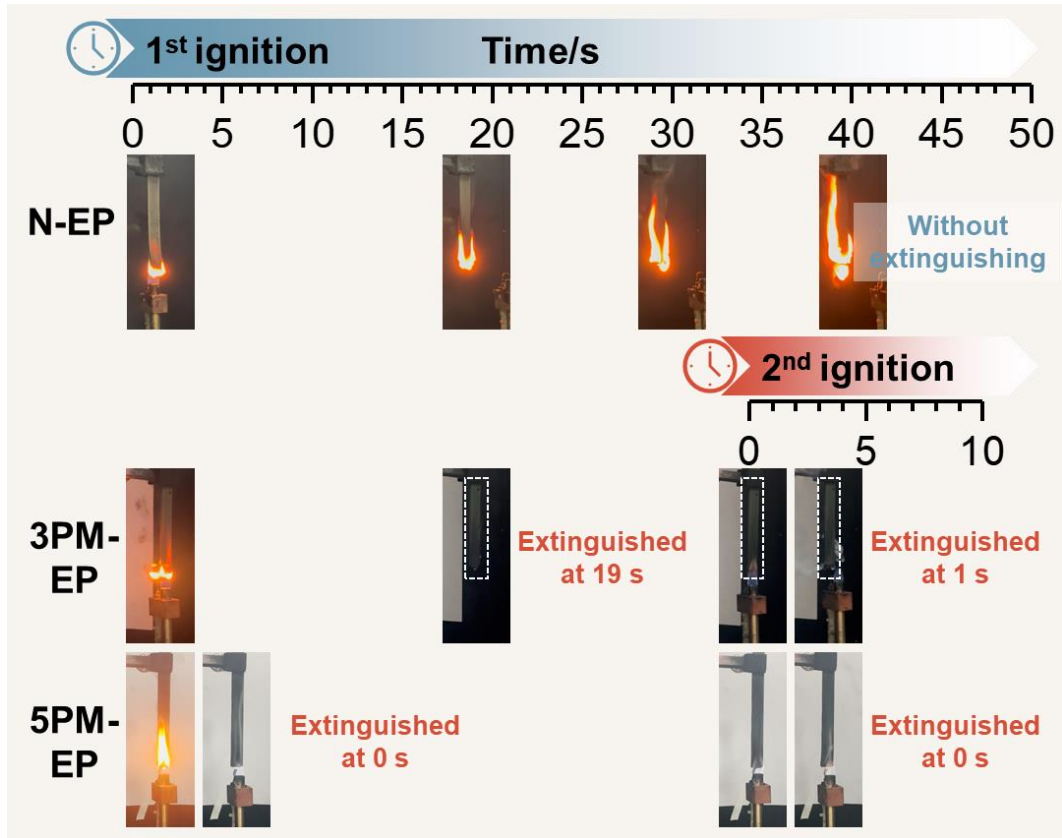
Figure S38. Combustion process of N-EP and PM-EP during the UL-94 test at different times.
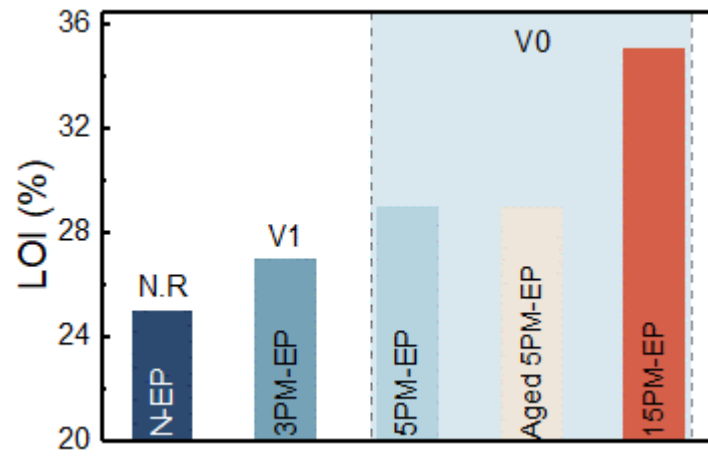
Figure S39. LOI values of PM-EP and aged PM-EP.
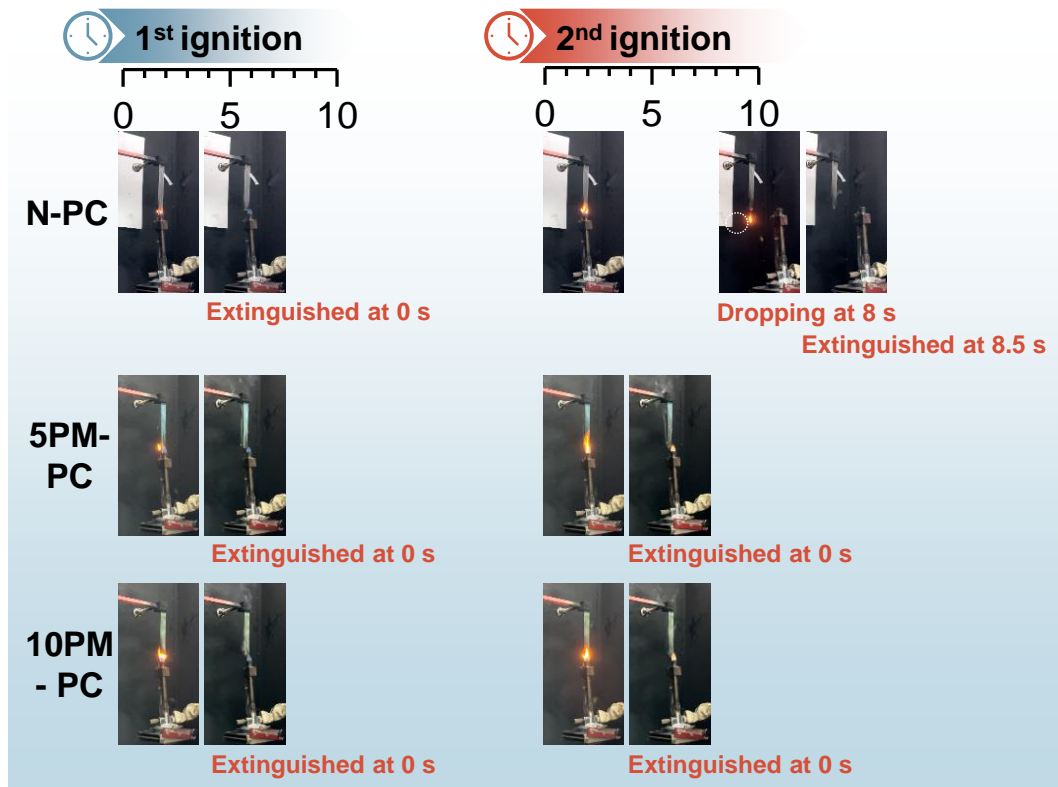
Figure S40. Combustion process of N-PC and PM-PC during the UL-94 test at different times.

3. Table S1-S10

Table S1. Elemental contents of PM, PM-N3, and PM-N6 acquired by EA and ICP–OES.

Sample	C wt%	H wt%	O wt%	P wt%	Cu wt%	P/Cu (Atom)
Theory	58.0	4.0	12.9	12.5	12.8	2.0
PM	57.06	4.06	14.00	11.37	12.1	1.92
PM-N3	52.00	3.87	17.13	10.43	15.69	1.36
PM-N6	50.24	3.86	17.40	10.32	15.86	1.33

Nitrolysis: PM was used as an example. PM (10 mg) and concentrated HNO_3 (10 mL) were added to a 100 mL beaker, the mixture was heated and concentrated to 1 mL, and then deionized water was added to 100 mL in a volumetric flask.

Table S2. Elemental contents of O, P, and Cu acquired by XPS.

Sample	O Atom%	P Atom%	Cu Atom%
Theory in PM	4	2	1
PM	56.8	30.7	12.6
PM-W6	60.5	≈0	39.5
PM-HN12	71.0	≈0	29.0
PM-HN25	66.2	≈0	33.8

Table S3. Binding energy of two PA molecules in H_2O and EtOH simulation systems.

Sample	Binding energy in water	Binding energy in ethanol
Interaction energy (kcal/mol)	-50.43	-37.82

Table S4. Formulations of N-F and flame-retardant foams with PM.

Sample	PM [a] (phb)	GEP-560s (phb)	L580 (phb)	H_2O (phb)	A33 (phb)	T9 (phb)	TDI (phb)
N-F	0	200	3.0	6.0	0.8	0.2	82
0.4PM-F	1.0	200	3.0	6.0	1.7	0.7	82
1.1PM-F	3.0	200	3.0	6.0	2.0	0.8	82
1.8PM-F	5.0	200	3.0	6.0	2.3	0.9	82
2.8PM-F	8.0	200	3.0	6.0	3.3	1.3	82

a) The unit of php represents parts per hundred units of polyether polyol by weight.

Table S5. Molecular weight characteristics and content of cupper/phosphorus in the recycled polyols obtained by glycolysis of N-F, PM-F, and vPM-F (virgin foam).

Characterization		GPC			ICP–OES [c]		
Sample	Catalysts	Mn (kDa)	Mw (kDa)	Đ	Cu (wt%)	P (wt%)	P/Cu [d]
Virgin polyols	/	2210	2594	1.17	/	/	/
PN-FK	1 wt%	3064	3439	1.12	0	0	/
PPM-FK	Potassium	4048	5437	1.34	< 0.05	< 0.01	0.41
PvPM-FK	propionate [b]	2960	3280	1.11	0	0	/
PN-F [a]		4156	5635	1.36	0	0	/
PPM-F	/	4029	5868	1.46	< 0.11	0.03	0.56
PvPM-F		4034	5693	1.41	0	0	/

a) Defined as a blank in the ICP–OES analysis for comparison. b) Related to the foam mass by weight. c) Theoretical weight percentages of copper and phosphorus are 0.484 wt% and 0.455 wt%, respectively. d) Ratio of atoms.

Table S6. Combustion parameters of N-F, PM-F, and aged PM-F collected from the vertical burning test and LOI test.

Sample	AFT[a)]/s		AGT[b)]/s	Char lengh/mm		Pass or fail	LOI (%)
	Ave.	Max.	Ave.	Ave.	Max		
Requirements for pass	≤ 5.0	≤ 15.0	≤ 15.0	≤ 152.4	≤ 203.2	Pass	/
N-F	-	-	0	-	-	No	18.0
0.4PM-F	-	-	0	-	-	No	/
1.1PM-F	1.8	4.0	0	45	60	Pass	20.5
1.8PM-F	0.0	1.0	0	24	32	Pass	21.0
Aged 1.8PM-F [c)]	0.0	0.0	0	26	30	Pass	21.0

a) and b) refer to the after-flame time and after-glow time, respectively. c) Conditions of hygrothermal aging resistance (according to GB/T 9640-2008): 100% RH, 105 °C for 3 h.

Table S7. Comparison of PM-F with other flame-retardant foams that can pass the vertical burning test in recent reports.

Flame retardant	Loading[b] (wt%)	P (wt%)	Density (kg/m^3)	Compression set (%)	Ref.
D-Mel	10	/	35	7.5	6
D-DICY	10	/	35	7.4	6
D-Urea	10	/	36	6.9	6
CMA	10	/	36	/	7
DPPMA	5	0.45	28	/	8
MPBT	10	/	/	12	9
EDPPA	10	/	/	/	10
EDPPO	20	/	/	/	10
EDPMA	20	/	/	/	10
DMMP	10	/	36	/	11
BDMPP	10	/	43	/	11
DMPMA	10	/	46	/	12
TPT	5	0.49	/	/	13
PDEO	10	/	37	/	14
DMOP	10	/	39	/	15
PPNs	5	0.32	43	2.3	16
DPM	2.5	0.33	33	7.1	17
TCDP	5	1.00	62	3.4	18
PM	**1.5**	**0.19**	**36**	**5.3**	**This work**

Table S8. Cone calorimetric data of N-F and PM-F at a heat radiation of 25 kW/m^2.

Sample	PHRR (kW/m^2)	THR (MJ/m^2)	TSP (m^2)
N-F	367	26.8	1.76
1.1PM-F	358	26.5	2.12
1.8PM-F	343	26.0	2.15

Table S9. TGA and DTG data for N-F and PM-F.

Sample	$T_{5\%}/$ (°C)	T_{max1} (°C)/ R_1 (%/min)	T_{max2} (°C)/ R_2 (%/min)	Residues (%)
PM	315.0	327/-5.0	405.0/-5.7	32.2
N-F	267.0	300/-6.7	377.0/-18.2	0.8
2.8PM-F	255.0	283.2/-5.40	374.6/-20.52	1.3

Table S10. Parameters of the compression resilience of N-F and PM-F.

Sample	Density (kg/m³)	σ (kPa)	ε (%)	δ (%)	ɵ (%)
N-F	34.7	4.37	95.46	99.42	6.0
0.4PM-F	34.1	4.73	95.77	97.24	6.6
1.8PM-F	37.7	5.98	94.31	98.32	5.3

σ, ε, δ, and ɵ refer to the compressive strength, strength recovery ratio, deformation recovery ratio, and compression set, respectively.

4. References

[1] Gaussian 09, Revision E.01, M. J. Frisch, G. W. Trucks, H. B. Schlegel, G. E. Scuseria, M. A. Robb, J. R. Cheeseman, G. Scalmani, V. Barone, B. Mennucci, G. A. Petersson, H. Nakatsuji, M. Caricato, X. Li, H. P. Hratchian, A. F. Izmaylov, J. Bloino, G. Zheng, J. L. Sonnenberg, M. Hada, M. Ehara, K. Toyota, R. Fukuda, J. Hasegawa, M. Ishida, T. Nakajima, Y. Honda, O. Kitao, H. Nakai, T. Vreven, J. A. Montgomery, Jr., J. E. Peralta, F. Ogliaro, M. Bearpark, J. J. Heyd, E. Brothers, K. N. Kudin, V. N. Staroverov, T. Keith, R. Kobayashi, J. Normand, K. Raghavachari, A. Rendell, J. C. Burant, S. S. Iyengar, J. Tomasi, M. Cossi, N. Rega, J. M. Millam, M. Klene, J. E. Knox, J. B. Cross, V. Bakken, C. Adamo, J. Jaramillo, R. Gomperts, R. E. Stratmann, O. Yazyev, A. J. Austin, R. Cammi, C. Pomelli, J. W. Ochterski, R. L. Martin, K. Morokuma, V. G. Zakrzewski, G. A. Voth, P. Salvador, J. J. Dannenberg, S. Dapprich, A. D. Daniels, O. Farkas, J. B. Foresman, J. V. Ortiz, J. Cioslowski, and D. J. Fox, Gaussian, Inc., Wallingford CT, **2013**.

[2] A. D. Becke, *J. Chem. Physics* **1993**, *98 (7)*, 5648-5652.

[3] C. Molero, A. de Lucas, J. F. Rodrı́guez, *Polym. Degrad. Stab.* **2006**, *91*, 221-228.

[4] C. H. Wu, C. Y. Chang, C. M. Cheng, H. C. Huang, *Polym. Degrad. Stab.* **2003**, *80*, 103-111.

[5] T. Vanbergen, I. Verlent, J. D. Geeter, B. Haelterman, L. Claes, D. D. Vos, *ChemSusChem* **2020**, *13*, 3835-3843.

[6] S. C. Ma, Y. L. Xiao, F. Zhou, B. Schartel, Y. Y. Chan, O. P. Korobeinichev, S. A. Trubachev, W. Z. Hu, C. Ma, Y. Hu, *Polym. Degrad. Stabil*. **2020**, *177*, 109160 (2020).

[7] M, J. Chen, Z, B. Shao, X. L. Wang, L. Chen, Y. Z. Wang, *Ind. Eng. Chem. Res*. **2012**, *51*, 9769-9776.

[8] W. H. Rao, Z. Y. Hu, H. X. Xu, Y. J. Xu, M. Qi, W. Liao, S. M. Xu, Y. Z. Wang, *Ind. Eng. Chem. Res*. **2017**, *56*, 7112-7119.

[9] S. Zhang, F. K. Chu, Z. M. Xu, Y. F. Zhou, Y. Qiu, L. J. Qian, Y. Hu, N. B. Wang, W. Z. Hu, *J. Colloid Interface Sci*. **2022**, *606*, 768-783.

[10] F. Zhou, C. Ma, K. Zhang, Y. Y. Chan, Y. L. Xiao, B. Schartel, M. Doring, B. B.

Wang, W. Z. Hu, Y. Hu, *Polym. Degrad. Stabil*. **2021**, *188*, 109557.

[11] F. Zhou, T. Zhang, B. Zou, W. Z. Hu, B. B. Wang, J. Zhan, C. Ma, Y. Hu, *Polym. Degrad. Stabil*. **2020**, *171*, 109029.

[12] C. Ma, K. Zhang, F. Zhou, Y. P. Zheng, W. R. Zeng, B. B. Wang, W. Y. Xing, W. Z. Hu, Y, *Polym. Degrad. Stabil*. **2021**, *189*, 109602.

[13] H. H. Zhou, S. Tan, G. H. Wang, Y. Wu, *Polym. Degrad. Stabil*. **2022**, *195*, 109789.

[14] W. H. Rao, Z. M. Zhu, S. X. Wang, T. Wang, Y. Tan, W. Liao, H. B. Zhao, Y. Z. Wang, *Polym. Degrad. Stabil*. **2018**, *153*, 192-200.

[15] W. H. Rao, H. X. Xu, Y. J. Xu, M. Qi, W. Liao, S. M. Xu, Y. Z. Wang, *Chem. Eng. J*. **2018**, *343*, 198-206.

[16] F. R. Zeng, B. W. Liu, Z. H. Wang, J. Y. Zhang, X. L. Chen, H. B. Zhao, Y. Z. Wang. *ACS Mater. Lett*. **2023**, *5*: 1692-1702.

[17] F. R. Zeng, X. F. Men, M. J. Chen, B. W. Liu, Q. W. Han, S. C. Huang, H. B. Zhao, Y. Z. Wang. *Chem. Eng. J*. **2023**, *454*: 140023.

[18] Z. C. Fu, F. Y. Bu, Z. P. Li, T. Wang, J. N. Deng, H. B. Zhao, S. C. Huang, Y. Z. Wang, M. J. Chen. *Chem. Eng. J*. **2024**, *454*: 147935.